References

Ahmed S.F.U., Maalej M. and Mihashi H. (2007). Cover cracking of reinforced concrete beams due to corrosion of steel. *ACI Mater. J.*, Vol. 1042, pp. 153-161.

Alonso C., Andradel C., Rodriguez J. and Diez J.M. (1998). Factors controlling cracking of concrete affected by reinforcement corrosion. *Materials and Structures,* 31, pp. 435-441.

Andrade C., Alonso C., and Molina F.J. (1993). Cover cracking as a function of bar corrosion: Part I-Experimental test. *Materials and Structures*, 26, pp. 453-464.

Bentur A., Diamon S. and Berke N.S. (1997). Steel corrosion in concrete. E&FN Spon.

Bolander J.E., Hong G.S. and Yoshitake K. (2000) Structural concrete analysis using rigid-body-spring networks. *Computer-Aided Civil and Infrastructure Engineering*, V. 15, pp.120-133.

Bolander J. E. and Saito S. (1998). Fracture analysis using spring network models with random geometry. *Engineering Fracture Mechanics*, 61, 569-591.

Cabrera J.G. (1996). Deterioration of concrete due to reinforcement steel corrosion. *Cement & Concrete Composites,* 18, pp.47-59.

Cundall P.A. and Strack O.D.L. (1979). A discrete numerical model for granular assemblies. *Geotechnique*, 29, pp. 47-65.

Ishikawa Y., Nakamura H. and Tanabe T. (2003). Development of crack propagation analysis by RBSM considering mass transfer, *Proceeding of JCI meeting*, *Japan Concrete Institute,* 25 (1), pp. 467-472 (in Japanese).

Kawai T. and Takeuchi N. (1990). Discrete limit analysis program, Series of limit analysis by computer 2. Tokyo: *Baifukan* (in Japanese).

Kawai T. (1977). New element models in discrete structural analysis. *Journal of the Society of Naval Architects of Japan*, 141, pp. 187-193.

Kawamura K., Tran K.K., Nakamura H. and Kunieda M. (2010). Surface crack propagation behavior against the surface deformation and inside cracks due to rebar corrosion. *Proceedings of Japan Concrete Institute annual meeting*. 32(1), pp. 1007-1012 (in Japanese).

Lundgren K. (2002). Modeling the effect of corrosion on bond in reinforced concrete, *Magazine of Concrete Research*. 54 (3), pp.165-173.

Maage M., Helland S., Poulsen E., Vennesland Ø. and Carlsen J.E. (1997). Service Life Prediction of Existing Concrete Structures Exposed to Marine Environment. *ACI Materials Journal*, 93, pp. 1-8.

Markeset I.G. and Myrdal R. (2008). Modeling of reinforcement corrosion in concrete - State of the art. Norway.

Maruya T., Hsu K., Takeda H. and Tangtermsirikul S. (2003). Numerical modeling of steel corrosion in concrete structures due to chloride ion, oxygen and water movement. *Journalo of Advanced Concrete Technology*. 1(2): pp.147-160.

Matsuo T., Nishiuchi T. and Matsumura T. (1997). Crack propagation analysis in concrete induced by rebar corrosion expansion, *Concrete Journal*, *Japan Concrete Institute,* 19, pp.99-104 (in Japanese).

Matsuo et al. (2008) Structural performance evaluation on aging underground reinforced concrete structures (in Japanese).

Murakami Y., Oshita H., Suzuki S. and Tsutsumi T (2008): Influence of stirrups and anchorage performance on residual strength of corroded RC beam. 64(4), pp. 631-649 (in Japanese).

Nagai K., Sato Y. and Ueda T. (2004). Mesoscopic simulation of failure of mortar and concrete by 2D RBSM. *Journal of Advanced Concrete Technology*. 2(3), pp. 359-374.

Nakamura H., Tran K. K., Kawamura K. and Kunieda M. (2010). Crack propagation analysis due to rebar corrosion. *Proceedings of the 7th International Conference on Fracture Mechanics of Concrete and Concrete Structures (FramCoS-7)*, Korea, pp. 921-928.

Nakamura H. and Higai T. (2001). Compressive fracture energy and fracture zone length of concrete, modeling of inelastic behavior of RC structures under seismic loads, *American Society of Civil Engineers*, 627 V-44, pp. 471-487.

Ngo D., Scordelis A. C. (1967). Finite element analysis of reinforced concrete. *ACI J* ,64, pp. 152-163.

Nguyen Q.T., Millard A., Care S., L'Hostis V. and Berthaud Y. (2006). Fracture of concrete caused by the reinforcement corrosion products. *J.Phys.IV France, 136, pp.* 109-120.

Oh B.H., Kim K.H. and Jang B.S. (2009). Critical corrosion amount to cause cracking of reinforced concrete structures. *ACI Material Journal*, 106 (4), pp.333-339.

Ohtsu M. and Yosimura S. (1997). Analysis of crack propagation and crack initiation due to corrosion of reinforcement. *Construction and Building Materials,* 11, Nos 7-8, pp. 437-442.

Ouglova A., François M., Berthaud Y., Caré S. and Foct F. (2006). Mechanical properties of an iron oxide formed by corrosion in reinforced concrete structures. *Corrosion Science* ,48, pp. 3988–4000.

Ravindra K.D., Harrison T. A., Zheng L. and Kandasami S. (2008). Concrete durability: achievement and enhancement. *Proceedings of the International Conference held at the University of Dundee, Scotland, UK.*

Saito S. (1999). Fracture analyses of structural concrete using spring network with random geometry. *Doctoral thesis*. Kyushu University.

Toongoenthong K. and Maekawa K. (2005).Simulation of coupled corrosive product formation, migration into crack and propagation in reinforced sections. *Journal of Advanced Concrete Technology,* 3(2), pp. 253-265.

Tran K. K., Kawamura K., Nakamura H. and Kunieda M. (2009). Prediction of cracking of concrete due to rebar corrosion using 3D- RBSM. *Proceedings of the Eleventh International Summer Symposium*, JSCE, pp. 249-252.

Tran K. K., Nakamura H., Kawamura K., and Kunieda M. (2010). Quantitatively evaluation of crack propagation due to rebar corrosion. *Proceedings of Japan Concrete Institute annual meeting*. 32(1), pp. 1043-1048.

Tran K. K., Nakamura H., Kawamura K. and Kunieda M. (2011) . Analysis of crack propagation due to rebar corrosion using RBSM. *Journal of Cement and Concrete Composites*. 33, pp. 906-917.

Tran K. K., Nakamura H., Kunieda M. and Ueda N. (2011). Three dimensional behavior of concrete cracking due to rebar corrosion, *Procedia Engineering,* Vol.(14), pp. 419-426.

Tsutsumi T., Matsushima M., Murakami Y. and Seki H. (1996). Study on crack models caused by pressure due to corrosion products, *Doboku Gakkai Ronbunshuu,* 30(2), pp. 159-166 (in Japanese).

Tullmin M. (2007). http://www.corrosion-club.com/concretecosts.htm

Ueda M., Kei T. and Taniguchi H. (1988). Discrete limit analysis of reinforced concrete structures by RBSM. *Proceedings of JCI*, 10 (3), pp. 335-338 (in Japanese).

Val V. D, Chernin L. and Stewart G. M. (2008). Experimental and numerical investigation of corrosion-induced cover cracking in reinforced concrete structures. *Journal of structural Engineering*, ASCE 2009; 135, pp. 376-385.

Wang L., Soda M., and Ueda T. (2008). Simulation of chloride diffusivity for cracked concrete based on RBSM and truss network model. J*ournal of Advanced Concrete Technology*; 6(1), pp.143-155.

Yamamoto T., Hattori A.. and Miyagawa T. (2002). Influence of reinforcing steel corrosion on flexural behavior of RC member confined with CFRP sheet. *Proceedings of the 1st FIB Congress.* Osaka, Japan 2002, pp. 177-182.

Yamamoto Y., Nakamura H., Kuroda I., and Furuya N. (2008). Analysis of compression failure of concrete by three dimensional rigid body spring model. *Doboku Gakkai Ronbunshuu,* 64(4), pp.612-630 (in Japanese).

Yanovich M., Thompson G. N., Balvanyos T. (2004). Appendix D Highway Bridges http://www.thermioninc.com/refmat-dot.php.

Yuan Y. and Ji Y. (2009). Modeling corroded section configuration of steel bar in concrete structure. *Construction and Building Materials*; 23(6), pp. 2461-2466.

A. Appendix A

APPLICABILITY OF RBSM METHOD IN SMALL MESH SPECIMENS

A.1. Introduction

In this study, specimen mesh sizes are relatively small. That is 5-10 mm meshes in the concrete cover thickness and 15-40 mm meshes on the other areas of the specimen. The relatively small meshes enable to observe crack propagation precisely in the concrete cover.

The applicability of the RBSM analytical method for small mesh size is calibrated and the proposed modifiers for the concrete properties parameters are given for the analysis as shown in **Table A.1**. The calibration of the RBSM model is conducted for several testes and the analytical results are verified against the test results. **Table A.1** shows parameter modifiers using in the analysis. In which, parameters for tensile behavior of normal springs are modified since the tensile behavior strongly depends on contact surface area of rigid body. So, the smaller mesh size will result larger contact surface area. Parameters for compressive behavior of normal springs and for shear behavior of shear springs are not modified.

Table A.1. **Parameter modifiers in the analysis**

Parameter	Modifier	Analytical value
G_F (N/mm)	0.505	**0.505***G_F
f_t (MPa)	0.850	**0.850***f_t
f'_c (MPa)	1.000	**1.000***f'_c
E_c (MPa)	1.000	**1.000***E_c

A.2. "Direct" tension test

The experiment was carried out by Cornelissen et al. (1986) to test a concrete specimen with double notches as shown in **Figure A**.1. The purpose to calibrate the analytical model in this specimen is that the tension behavior of concrete is dominant in the case of corrosion induced expansion (Lundgren, 2002; Nguyen et al., 2006). This calibration is to verify the proposed modified parameters as mentioned above.

The specimen was simulated with the 5mm meshes around the notches and 15 mm in the other areas as shown in **Figure A.2**. The concrete properties parameters used in the analysis are determined from the parameter modifiers in **Table A.1**. The analytical results including the relationship of average displacement of the 35mm- gauges and the tension stress σ (MPa) and the 3D deformation of the specimen were compared with the test results as shown in **Figure A**.3. The analytical results appear reasonable agreement for tensile strength and post peak behavior Crack patterns are also understood from the deformation, because the deformation is occurred by the separation between rigid bodies in RBSM. The reasonable crack patterns and propagation behavior are simulated.

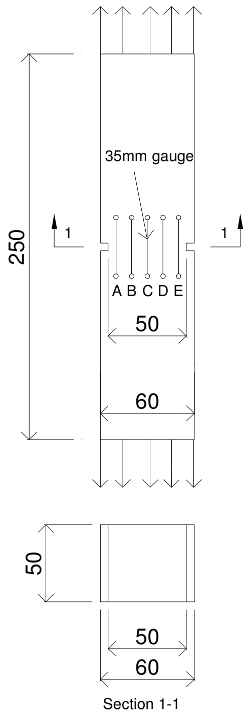

Parameter	Experimental value	Analytical value
G_f (N/mm)	0.103	**0.052**
f_t (MPa)	3.2	**2.720**
f'_c (MPa)	50	**50.00**
E_c (MPa)	3.93E+04	**3.93E+04**

Figure A.1. Outline of "direct" tension test

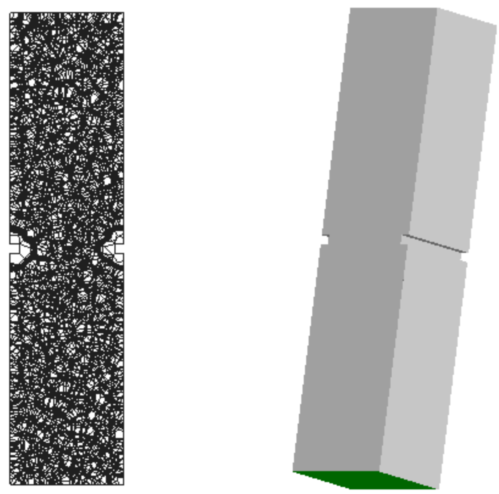

Figure A.2. RBSM modeling of "direct" tension specimen

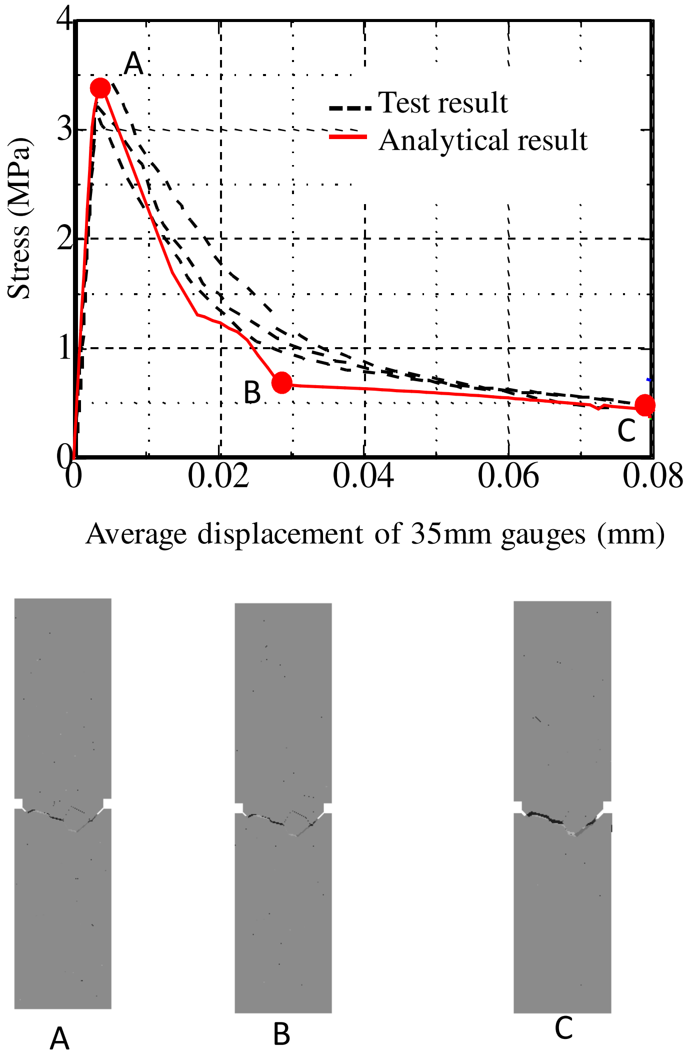

Deformation after peak regime
(magnification = 25)

Figure A.3. Analytical results of "direct" tension specimen

A.3. Pre-cracked three-point bending test

In order to calibrate the RBSM analytical model in the bending test, pre-cracked three-point bending beams with a 3 mm wide pre-crack are loaded. The set-up of the beam is shown in the **Figure A.4**. The purpose to calibrate the analytical model in this specimen is to verify the crack propagation under the bending behavior of concrete because a specimen tends to be bent in the case of rebar corrosion induced expansion (Nguyen et al., 2006). This calibration is to verify the proposed modified parameters as mentioned above.

The specimen was simulated with 5 mm meshes around the pre-crack and 10 mm in the other areas as shown in **Figure A.5**. The parameters used in the analysis are shown in **Figure A.4**. The relationship between the load and the CMOD (Crack Mouth Opening Displacement) obtained from the analysis is compared with the test results in **Figure A.6**. The 3D deformation of the beam showing crack patterns at small and large CMOD values is also shown in **Figure A.6**. The analytical results appear well agreement with the test results in both pre-peak and post-peak regimes. Especially, the applicability to large CMOD value, which is larger than 1 mm, is confirmed.

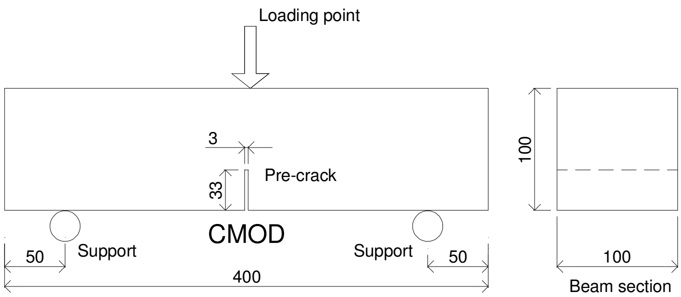

Parameters	Experimental value	Analytical value
G_f (N/mm)	0.091	**0.046**
f_t (MPa)	3.122	**2.654**
f'_c (MPa)	50	**50.000**
E_c (MPa)	3.32E+04	**3.32E+04**

Figure A.4. Set-up of pre-cracked three point bending specimen

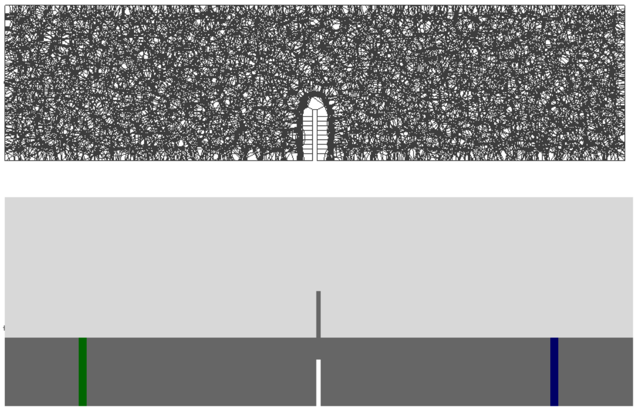

Figure A.5. Meshing of pre-cracked 3- point bending test

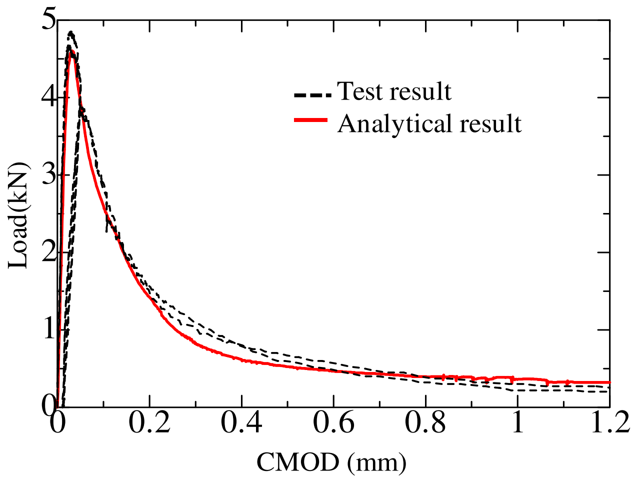

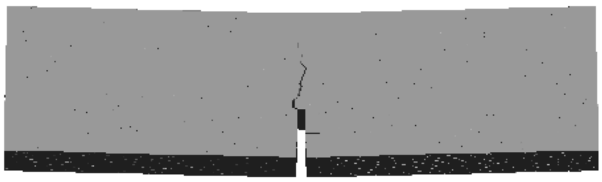

Deformation @CMOD = **0.05 mm**
Magnification =60

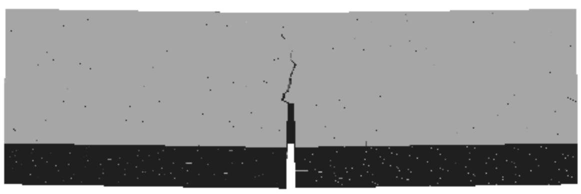

Deformation @CMOD = **1.00 mm**
Magnification =3

Figure A.6. Analytical results of pre-cracked three point bending test

A.4. Cylinder compression test

Although compressive behavior does not directly occur in the case of corrosion induced expansion specimen, the shear behavior can be verified in the compression test since the shear behavior is dominant in meso-level for compression failure. This validation is to verify the assumed shear parameters as mentioned in the concrete model.

Watanabe and Niwa (2004) carried out a compression test for a ϕ100*200 mm cylinder concrete with concrete properties used in the analysis as shown in **Figure A.7**. The specimen is modeled with a unique 10 mm mesh size as shown **Figure A.8**. The stress-strain relationship obtained from the analysis is compared with the test results as shown in **Figure A.9**. Again, the analytical results reasonably agree with the test results.

The above verifications against the various specimen tests show the applicability of the RBSM analytical model in concrete structural analysis for small mesh size less than 10 mm.

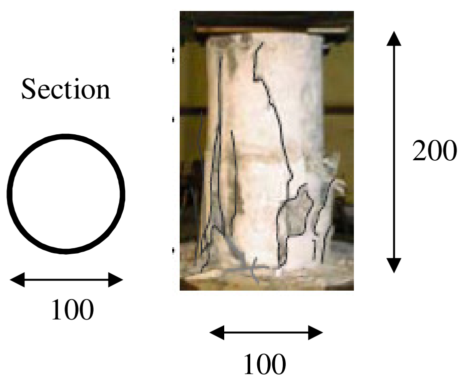

Parameter	Experimental value	Analytical value
G_f (N/mm)	0.078	**0.039**
f_t (MPa)	2.28	**1.933**
f'_c (MPa)	31.10	**31.10**
E_c (MPa)	2.62E+04	**2.62E+4**

Figure A.7. Set-up of cylinder compression test

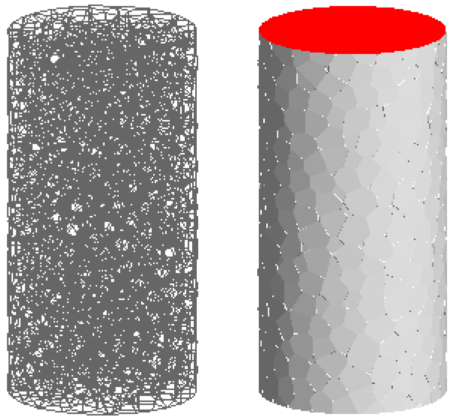

Figure A.8. RSBM modeling of compression cylinder

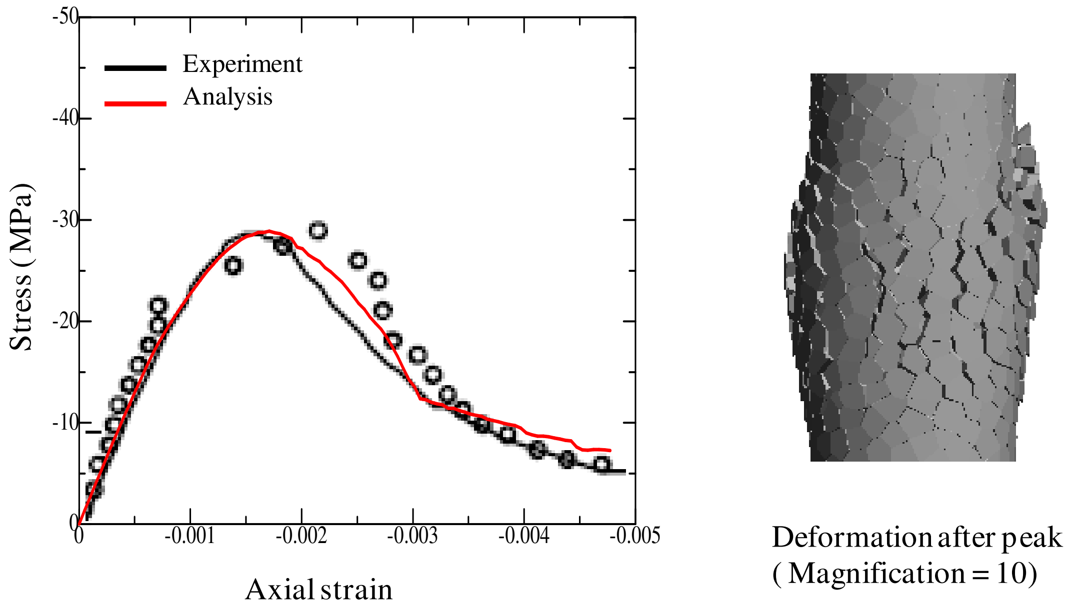

Figure A.9. Analytical results of cylinder compression specimen

B. Appendix B

EXPERIMENTAL RESULTS

B.1. Introduction

In appendix B, the experimental results of the specimen series conducted in this study are presented.

B.2. Specimen series 150*150-C30

B.2.1. Surface crack propagation

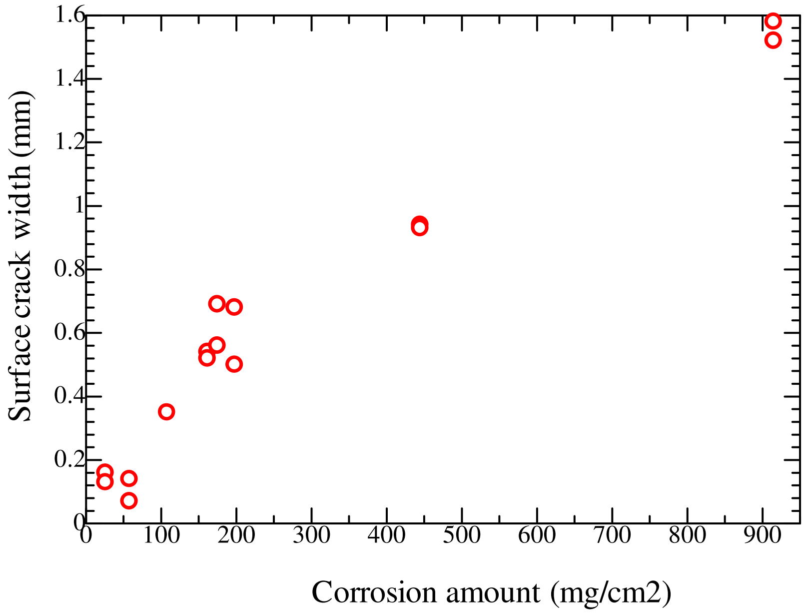

Figure B.1. Surface crack width propagation of 150*150-C30

B.2.2. Surface crack pattern

Corrosion amount: 445 mg/cm^2
Surface crack width: 0.94 mm, 0.93 mm

Figure B.2. Typical notation on crack patterns

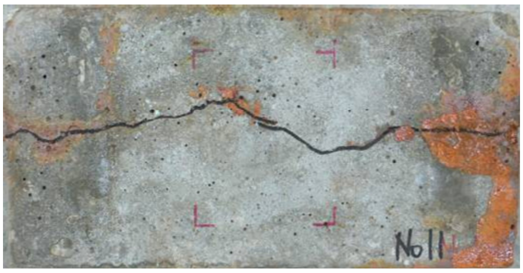

162 mg/cm^2

0.54 mm, 0.52 mm

198 mg/cm^2

0.50 mm, 0.68 mm

445 mg/cm^2

0.94 mm, 0.93 mm

915 mg/cm^2

1.52 mm, 1.58 mm

Figure B.3. Surface crack patterns of 150*150-C30

B.2.3. Internal crack pattern

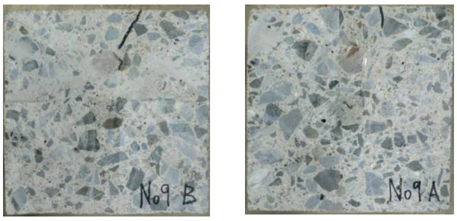

26 mg/cm^2

0.16 mm, 0.13 mm

58 mg/cm^2

0.07 mm, 0.14 mm

108 mg/cm^2

0.35 mm

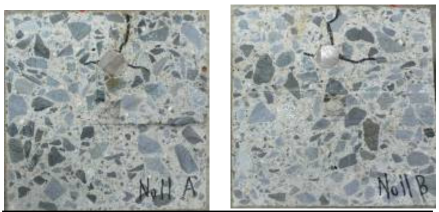

162 mg/cm^2

0.54 mm, 0.52 mm

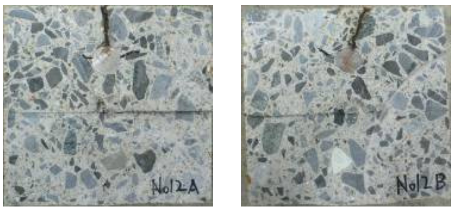

175 mg/cm^2

0.69 mm, 0.56 mm

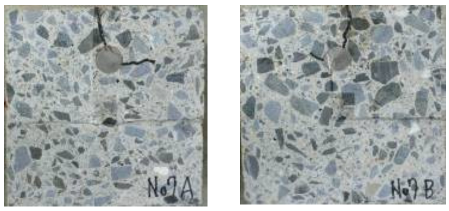

198 mg/cm^2

0.50 mm, 0.68 mm

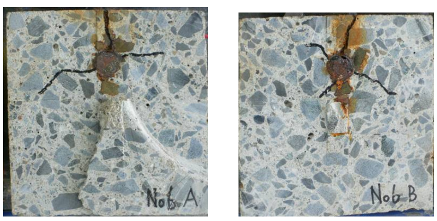

445 mg/cm^2

0.94 mm, 0.93 mm

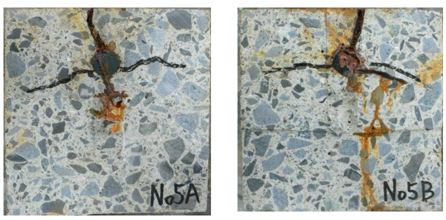

915 mg/cm^2

1.52 mm, 1.58 mm

Figure B.4. Internal crack patterns of 150*150-C30

B.2.4. Actual rebar corroded sectional pattern

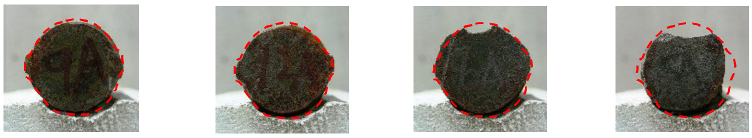

26 mg/cm^2 175mg/cm^2 445 mg/cm^2 915 mg/cm^2

Figure B.5. Actual rebar corroded sectional pattern of 150*150-C30

B.3. Specimen series 150*150-C7.5

B.3.1. Internal crack pattern

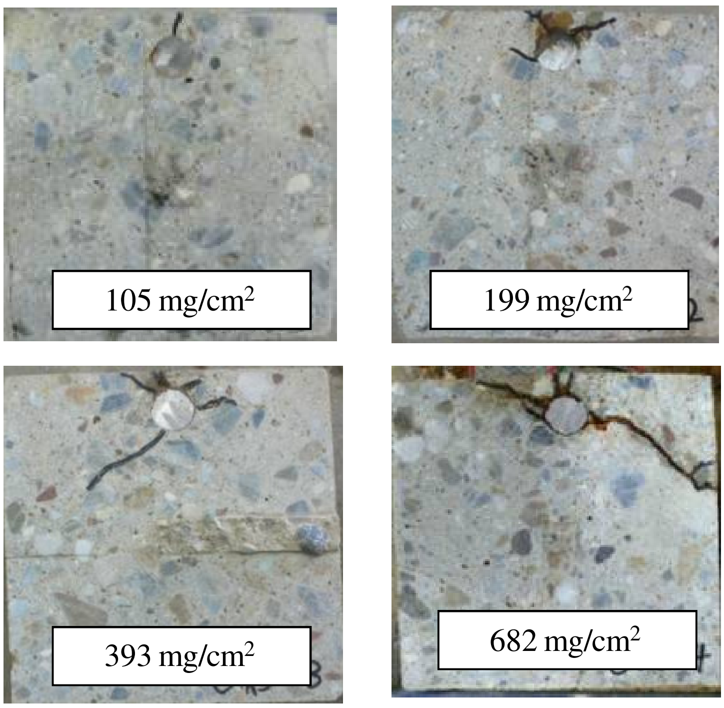

Figure B.6. Internal crack pattern of 150*150-C7.5

B.3.2. Actual rebar corroded sectional pattern

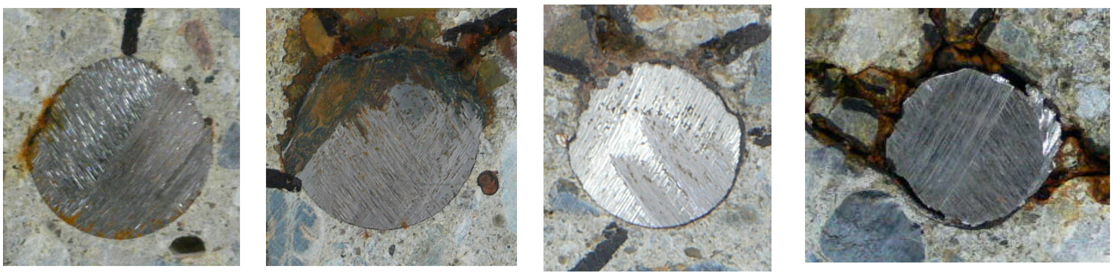

105 mg/cm^2 | 199 mg/cm^2 | 393 mg/cm^2 | 682 mg/cm^2

Figure B.7. Actual rebar corroded sectional pattern of 150*150-C7.5

B.4. Specimen series 150*150-C15

B.4.1. Surface crack propagation

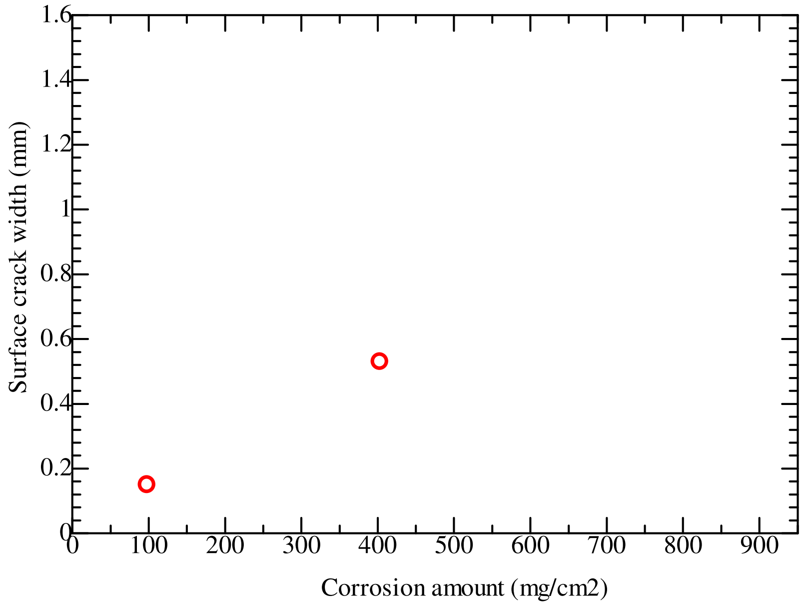

Figure B.8. Surface crack width propagation of 150*150-C15

B.4.2. Surface crack pattern

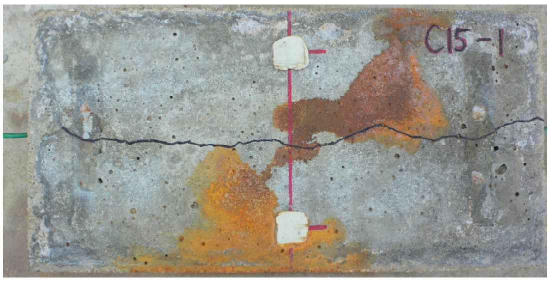

98 mg/cm²

0.15 mm

185 mg/cm²

403 mg/cm²

0.53 mm

770 mg/cm²

Figure B.9. Surface crack patterns of 150*150-C15

B.4.3. Internal crack pattern

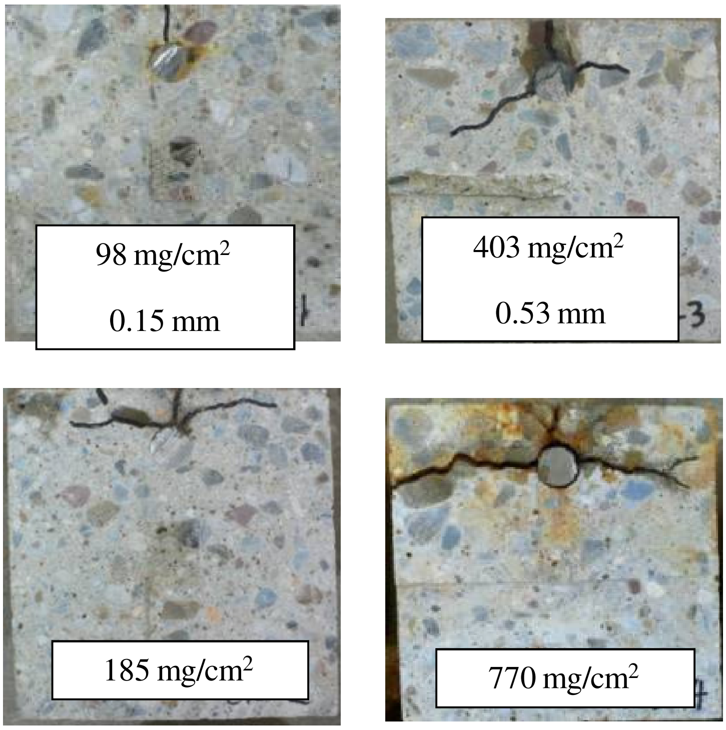

Figure B.10. Internal crack patterns of 150*150-C15

B.4.4. Actual rebar corroded sectional pattern

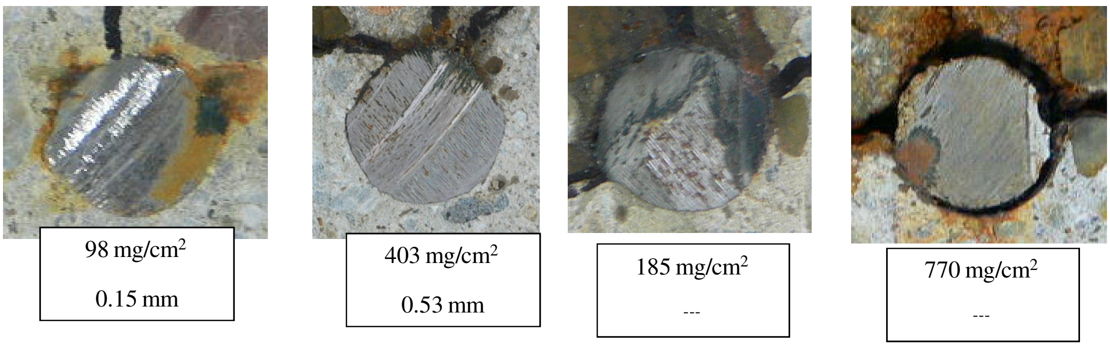

Figure B.11. Actual rebar corroded sectional pattern of 150*150-C15

B.5. Specimen series 150*150-C45

B.5.1. Surface crack propagation

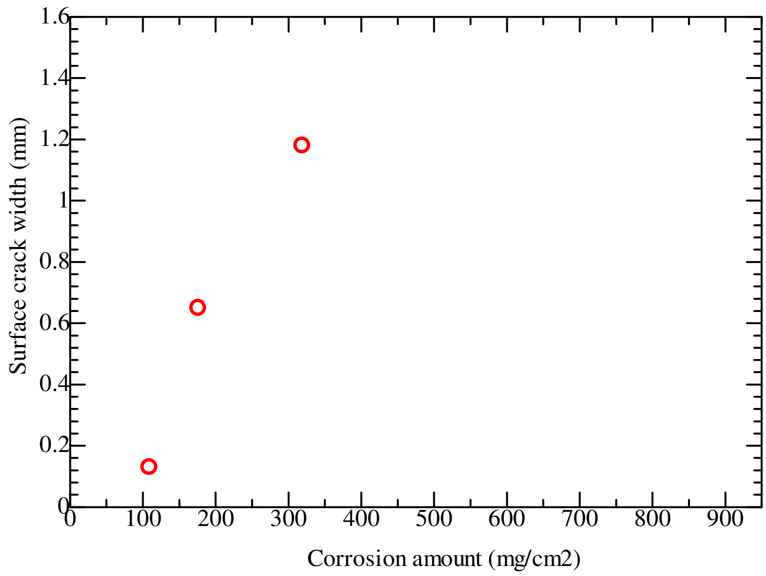

Figure B.12. Surface crack width propagation of 150*150-C45

B.5.2. Surface crack pattern

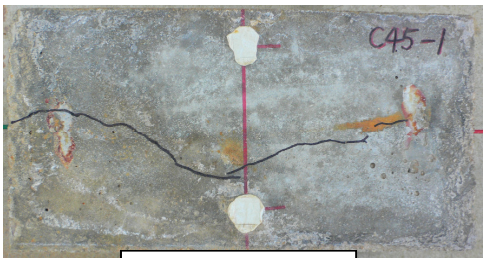

109 mg/cm^2

0.13 mm

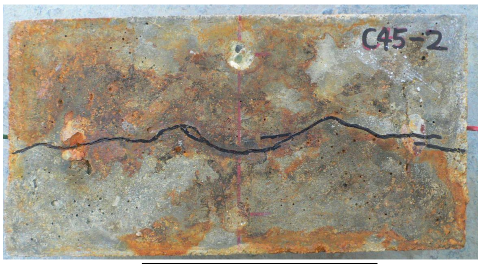

176 mg/cm^2

0.65 mm

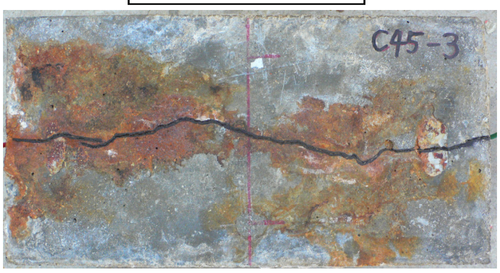

319 mg/cm^2

1.18 mm

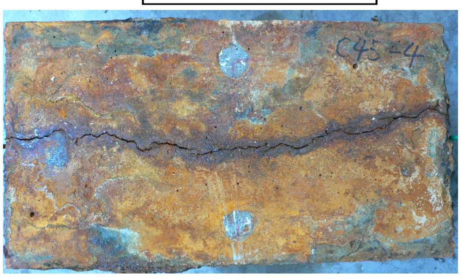

526 mg/cm^2

1.84 mm

Figure B.13. Surface crack patterns of 150*150-C45

B.5.3. Internal crack pattern

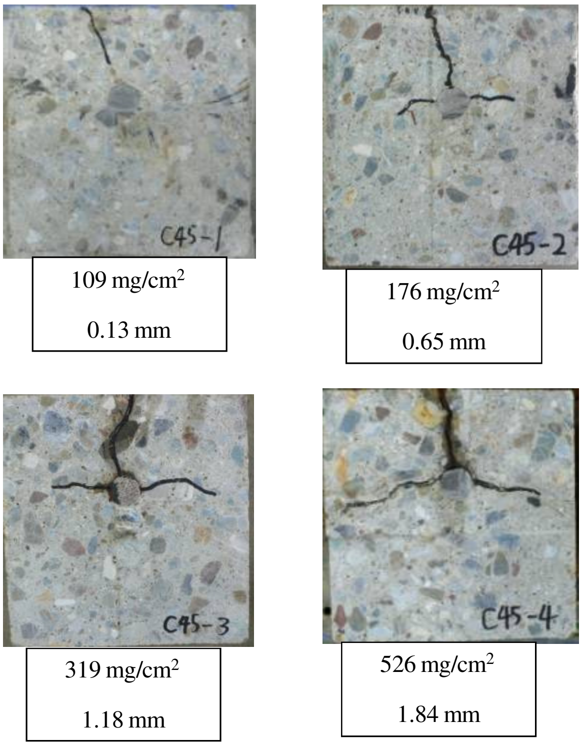

Figure B.14. Internal crack patterns of 150*150-C45

B.5.4. Actual rebar corroded sectional pattern

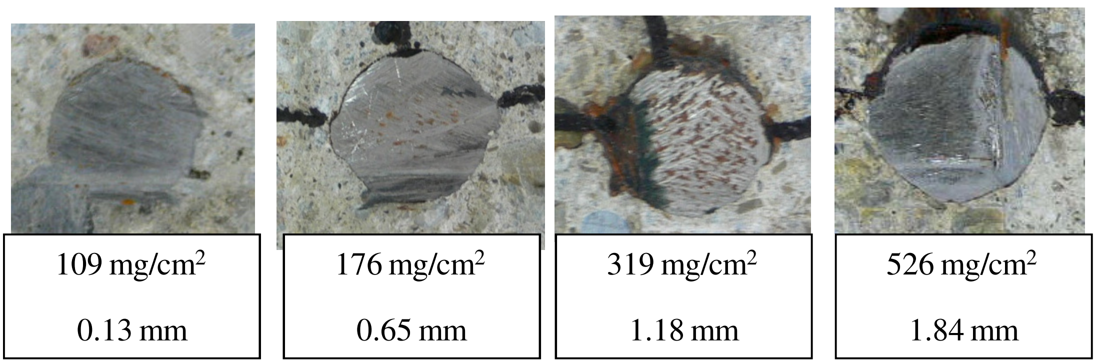

Figure B.15. Actual rebar corroded sectional pattern of 150*150-C45

B.6. Specimen series 150*150-D10

B.6.1. Surface crack propagation

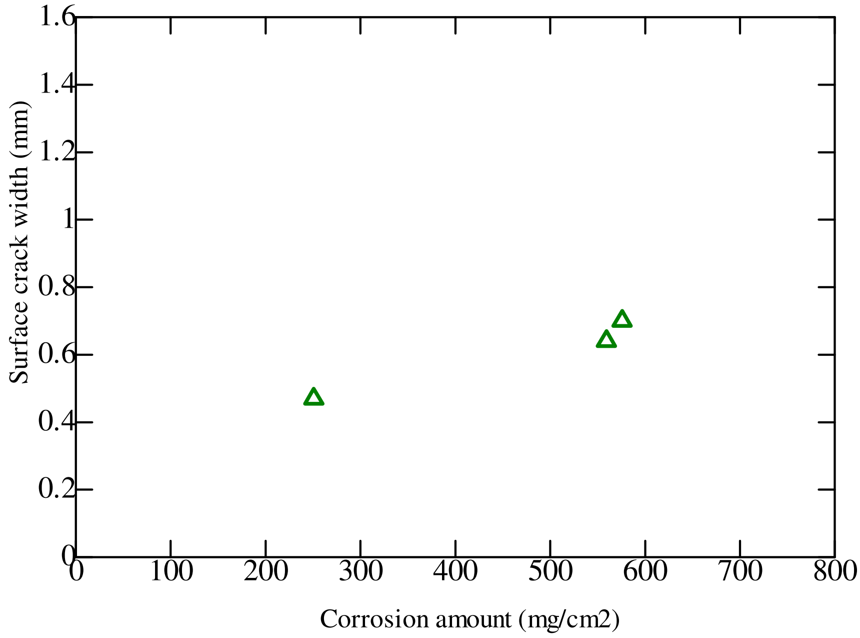

Figure B.16. Surface crack width propagation of 150*150-D10

B.6.2. Surface crack pattern

575.73 mg/cm^2
0.64 mm

250.60 mg/cm^2
0.47 mm

559.20 mg/cm^2
0.61 mm

Figure B.17. Surface crack patterns of 150*150-D10

B.6.3. *Internal crack pattern*

250.60 mg/cm^2
0.47 mm

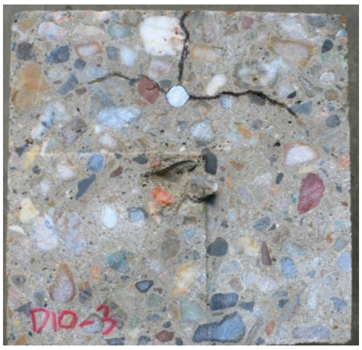

559.20 mg/cm^2
0.61mm

575.73 mg/cm^2
0.64mm

Figure B.18. Internal crack patterns of 150*150-D10

B.6.4. *Actual rebar corroded sectional pattern*

250.60 mg/cm^2 0.47 mm	559.20 mg/cm^2 0.61 mm	575.73 mg/cm^2 0.64 mm

Figure B.19. Actual rebar corroded sectional pattern of 150*150-D10

B.7. Specimen series 150*150-D25

B.7.1. *Surface crack propagation*

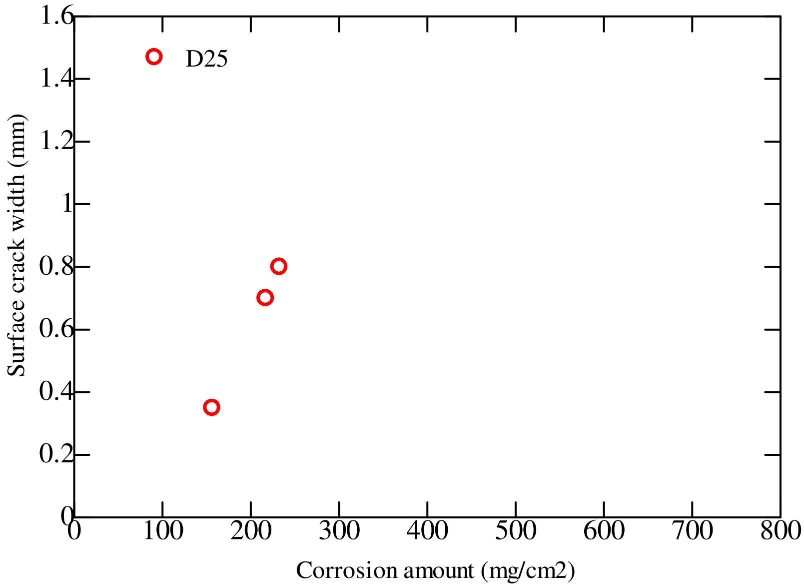

Figure B.20. Surface crack width propagation of 150*150-D25

B.7.2. *Surface crack pattern*

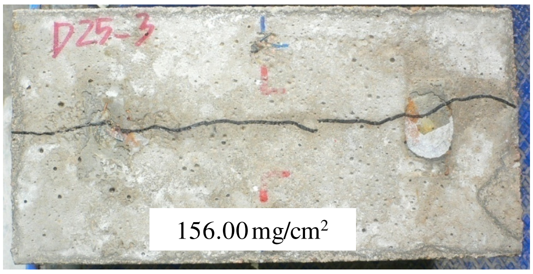

156 mg/cm²

0.35 mm

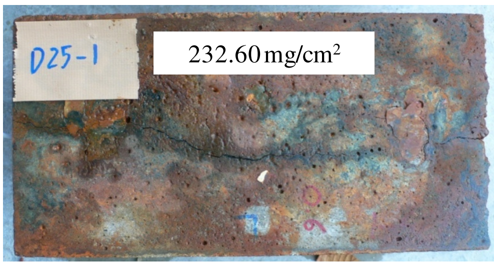

232 mg/cm²

0.8 mm

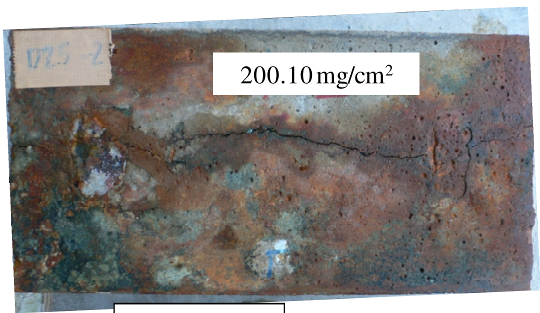

200 mg/cm²

0.7 mm

Figure B.21. Surface crack patterns of 150*150-D25

B.7.3. Internal crack pattern

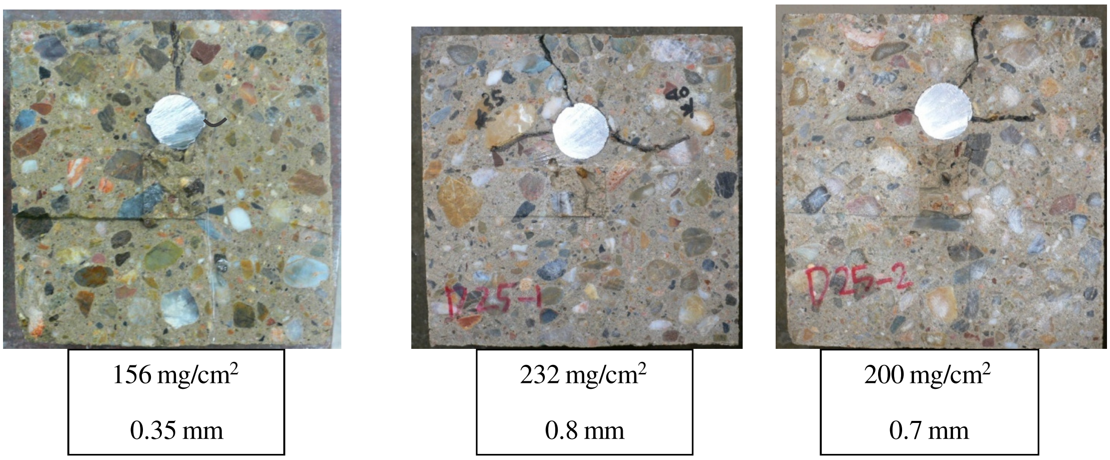

Figure B.22. Internal crack patterns of 150*150-D25

B.7.4. Actual rebar corroded sectional pattern

Figure B.23. Actual rebar corroded sectional pattern of 150*150-D25

B.8. Specimen series 300*150-C30

B.8.1. Surface crack propagation

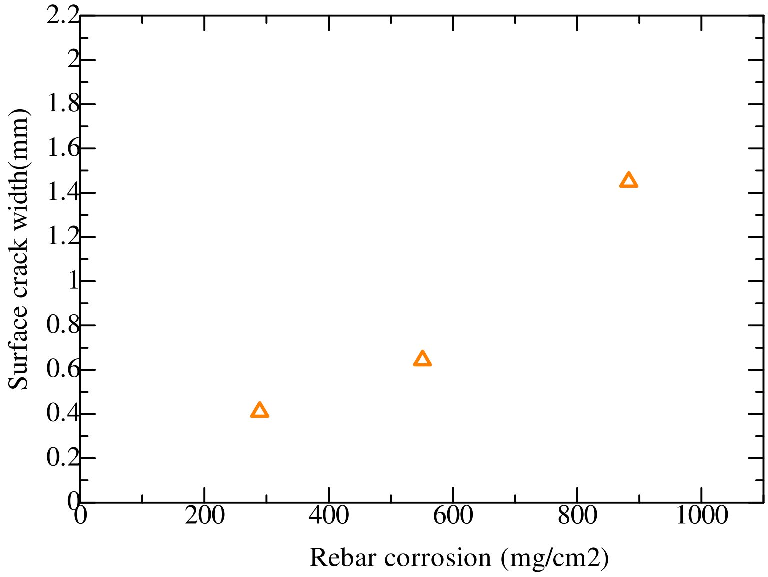

Figure B.24. Surface crack width propagation of 300*150-C25

B.8.2. Surface crack pattern

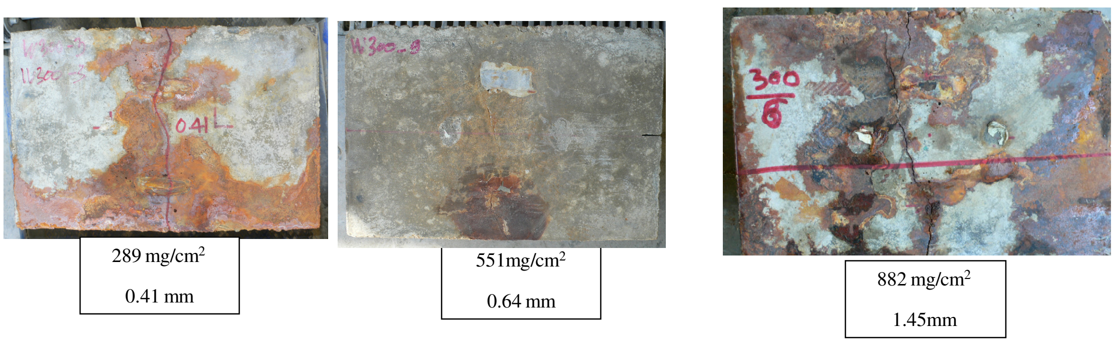

Figure B.25. Surface crack patterns of 300*150-C30

B.8.3. Internal crack pattern

289 mg/cm²

0.41 mm

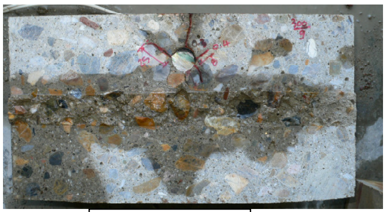

551mg/cm²

0.64 mm

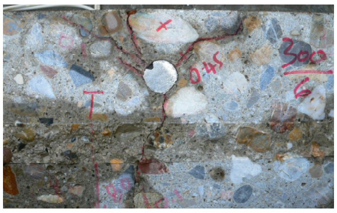

882 mg/cm²

1.45mm

Figure B.26. Internal crack patterns of 300*150-C30

B.8.4. Actual rebar corroded sectional pattern

289 mg/cm²

0.41 mm

551mg/cm²

0.64 mm

882 mg/cm²

1.45mm

Figure B.27. Actual rebar corroded sectional pattern of 300*150-C30

B.9. Specimen series 250*250-C30

B.9.1. Surface crack propagation

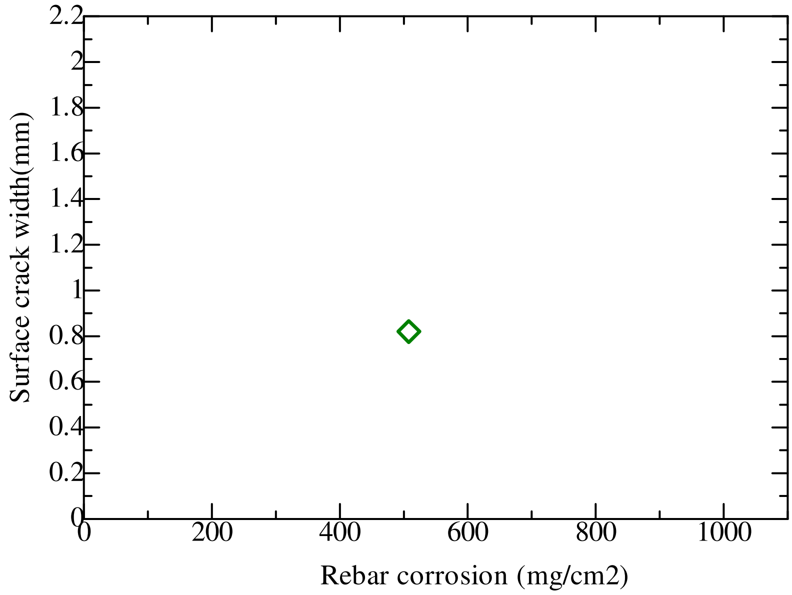

Figure B.28. Surface crack width propagation of 250*250-C30

B.9.2. Surface crack pattern

508 mg/cm^2
0.82 mm

Figure B.29. Surface crack pattern of 250*250-C30

B.9.3. Internal crack pattern

508 mg/cm^2

0.82 mm

Figure B.30. Internal crack pattern of 250*250-C30

B.9.4. Actual rebar corroded sectional pattern

508 mg/cm^2

0.82 mm

Figure B.31. Actual rebar corroded sectional pattern of 250*250-C30

B.10. Specimen series 400*400-C30

B.10.1. Surface crack propagation

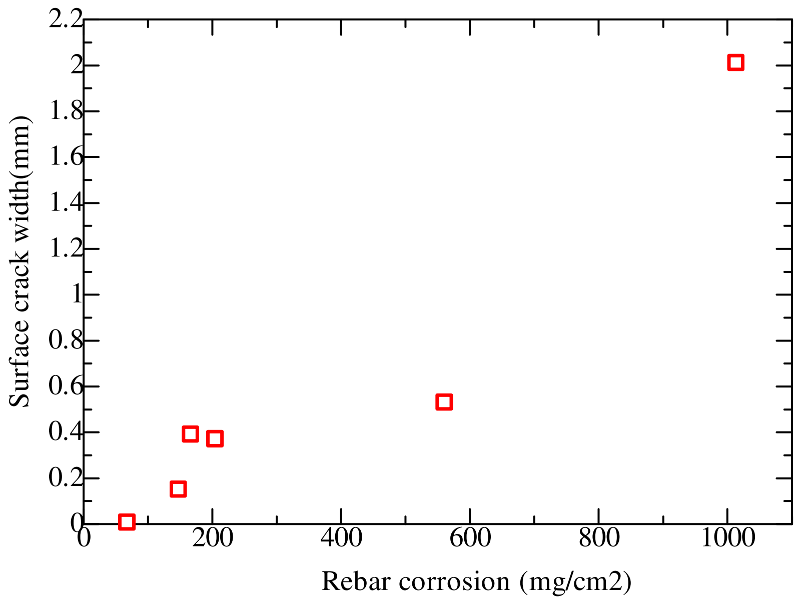

Figure B.32. Surface crack width propagation of 400*400-C30

B.10.2. Surface crack pattern

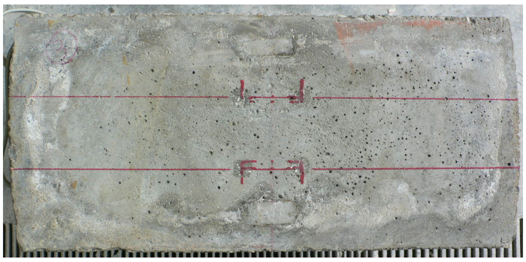

147 mg/cm^2

0.15 mm

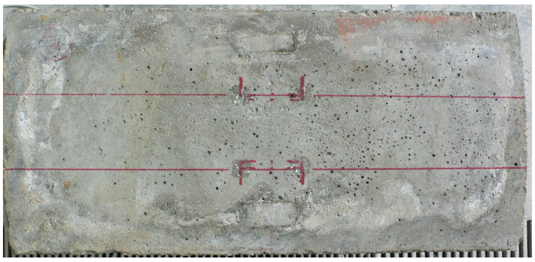

560 mg/cm^2

0.53 mm

167mg/cm^2

0.39 mm

1014 mg/cm^2

2.01 mm

167mg/cm^2

0.39 mm

1014 mg/cm^2

2.01 mm

Figure B.33. Surface crack pattern of 400*400-C30

B.10.3. Internal crack pattern

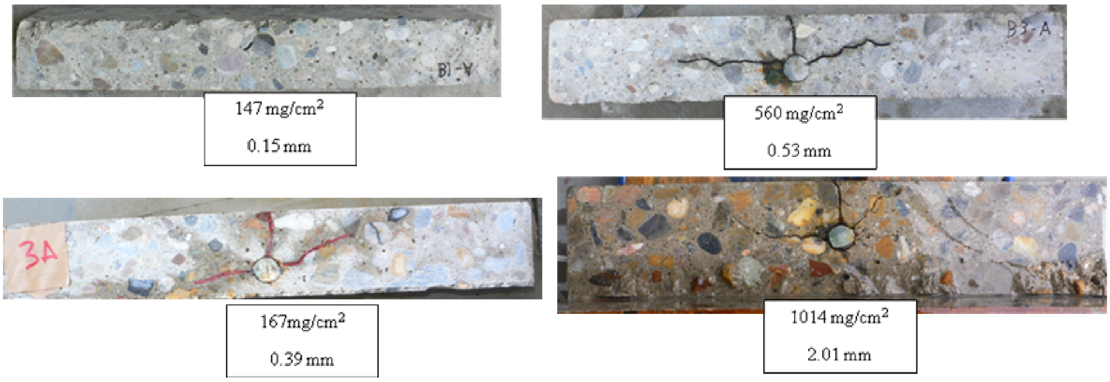

Figure B.34. Internal crack pattern of 400*400-C30

B.10.4. Actual rebar corroded sectional pattern

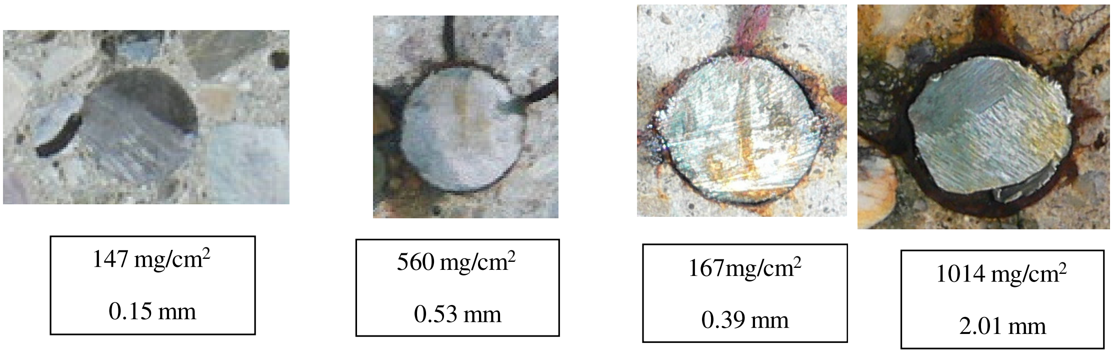

Figure B.35. Actual rebar corroded sectional pattern of 400*400-C30

B.11. Specimen series 600*400-C30

B.11.1. Surface crack propagation

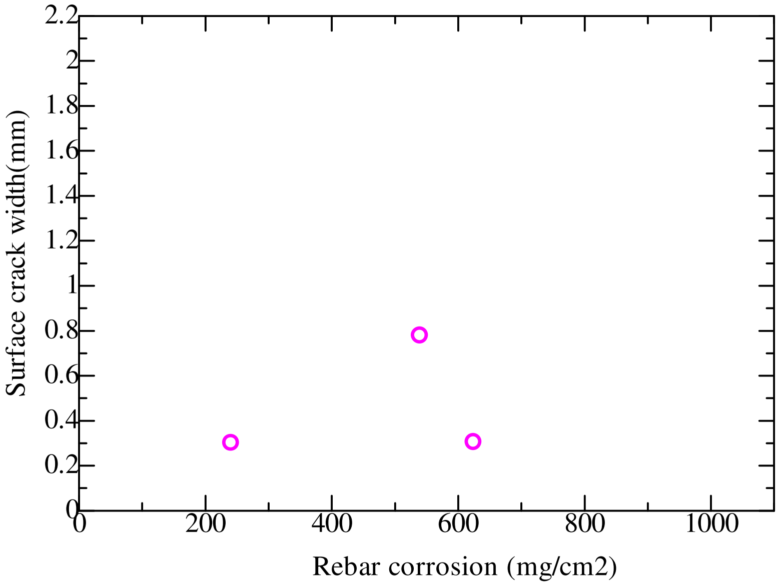

Figure B.36. Surface crack width propagation of 600*400-C30

B.11.2. Surface crack pattern

240 mg/cm²
0.30 mm

539 mg/cm²
0.70 mm (middle)

624mg/cm²
0. 30mm (middle)

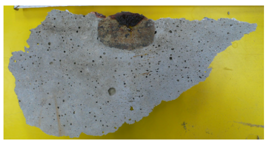

Figure B.37. Surface crack pattern of 600*400-C30

B.11.3. Internal crack pattern

240 mg/cm^2
0.30 mm

539 mg/cm^2
0.70 mm (middle)

624mg/cm^2
0. 30mm (middle)

Figure B.38. Internal crack pattern of 600*400-C30

B.11.4. Actual rebar corroded sectional pattern

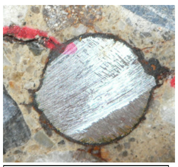

240 mg/cm^2
0.30 mm

539 mg/cm^2
0.70 mm (middle)

624mg/cm^2
0. 30mm (middle)

Figure B.39. Actual rebar corroded sectional pattern of 600*400-C30